J. Fluid Mech. (2012), *vol.* 702, *pp.* 378–402. © Cambridge University Press 2012
doi:10.1017/jfm.2012.184

Global stability of multiple solutions in plane sudden-expansion flow

Daniel Lanzerstorfer and Hendrik C. Kuhlmann†

Institute of Fluid Mechanics and Heat Transfer, Vienna University of Technology, Resselgasse 3, A-1040 Vienna, Austria

(Received 15 December 2011; revised 7 March 2012; accepted 12 April 2012; first published online 16 May 2012)

The two-dimensional, incompressible flow in a plane sudden expansion is investigated numerically for a systematic variation of the geometry, covering expansion ratios (steps-to-outlet heights) from 0.25 to 0.95. By means of a three-dimensional linear stability analysis global temporal modes are scrutinized. In a symmetric expansion the primary bifurcation is stationary and two-dimensional, breaking the mirror symmetry with respect to the mid-plane. The secondary asymmetric flow experiences a secondary instability to different three-dimensional modes, depending on the expansion ratio. For a moderately asymmetric expansion only one of the two secondary flows (the connected branch) is realized at low Reynolds numbers. Since the perturbed secondary flow does not deviate much from the symmetric secondary flow, both secondary stability boundaries are very close to each other. For very small and very large expansion ratios an asymptotic behaviour is found for suitably scaled critical Reynolds numbers and wavenumbers. Representative instabilities are analysed in detail using an *a posteriori* energy transfer analysis to reveal the physical nature of the instabilities. Depending on the geometry, pure centrifugal and elliptical amplification processes are identified. We also find that the basic flow can become unstable due to the effects of flow deceleration, streamline convergence and high shear stresses, respectively.

Key words: instability, transition to turbulence

1. Introduction

The steady laminar two-dimensional flow of an incompressible Newtonian fluid though a channel with a symmetric sudden expansion can either be symmetric or asymmetric with respect to the plane of symmetry, depending on the Reynolds number. Experiments of Durst, Melling & Whitelaw (1974), Cherdron, Durst & Whitelaw (1978), Sobey & Drazin (1986), Fearn, Mullin & Cliffe (1990) and Durst, Pereira & Tropea (1993) have shown that the primary flow is steady, two-dimensional and symmetric, with two recirculation zones of equal size near the expansion corners if the expansion ratio is moderate and the Reynolds number Re is sufficiently small. The length of the separation zones increases linearly with the Reynolds number. At higher Re, however, the flow loses its symmetry with respect to the mid-plane, and a pair of stable, steady, two-dimensional asymmetric flow states evolves gradually with recirculation zones of various lengths.

† Email address for correspondence: h.kuhlmann@tuwien.ac.at

https://doi.org/10.1017/jfm.2012.184 Published online by Cambridge University Press

Using experimental and numerical techniques, Fearn *et al.* (1990) demonstrated that the symmetric solution (primary flow) becomes unstable at a primary critical Reynolds number, and a pair of stable, asymmetric solutions (secondary flow) bifurcates supercritically. The slightly imperfect bifurcation found experimentally by Fearn *et al.* (1990) was modelled numerically by introducing a slightly asymmetric expansion in the computational geometry.

The linear stability analyses of Shapira & Degani (1990) and Alleborn *et al.* (1997) for a symmetric channel geometry revealed that the symmetric primary flow is stable for $Re \leqslant Re_c$ with respect to two-dimensional perturbations. At higher Reynolds numbers, however, it loses its stability via a symmetric pitchfork bifurcation, and two stable, asymmetric secondary flow states evolve. This result was confirmed by Rusak & Hawa (1999) by use of a weakly nonlinear analysis of the unsteady Navier–Stokes equations for $|Re - Re_c|/Re \ll 1$. The two-dimensional, time-dependent simulations of Hawa & Rusak (2001) established the relationship between the neutral modes of the linear stability analysis and the nonlinear time-asymptotic secondary flow. The asymptotic analysis of Rusak & Hawa (1999) was extended by Hawa & Rusak (2000) by considering a slightly asymmetric expansion. Above a certain threshold Reynolds number, three asymmetric solutions were found to exist: a stable solution branch continuously evolving out of the primary flow and two disconnected solutions, one stable and the other unstable, which are created through a saddle-node bifurcation. The contiguous smooth solution branch of the imperfect pitchfork bifurcation showed close agreement with the experimental data of Fearn *et al.* (1990), whereas the stable saddle-node branch did not agree well with the corresponding unperturbed secondary flow. These results were confirmed by Mizushima & Shiotani (2000) in their weakly nonlinear stability analysis for a slightly imperfect channel geometry.

Three-dimensional, time-dependent simulations were performed by Chiang, Sheu & Wang (2000), Schreck & Schäfer (2000), Chiang *et al.* (2001) and Tsui & Wang (2008), taking into account the finite spanwise extent of the channel. Schreck & Schäfer (2000) reported that narrower channel depths, i.e. smaller spanwise aspect ratios, decrease the lengths of the recirculation zones and stabilize the primary symmetric and nominally two-dimensional flow, which was also observed experimentally by Cherdron *et al.* (1978). Chiang *et al.* (2000) also studied the side-wall effects on the structure of the laminar flow for various spanwise aspect ratios $\Lambda = d/h_i$, i.e. depth-to-height of the inflow channel. They reported that the two-dimensional results differ considerably from the three-dimensional ones for $\Lambda \leqslant 12$. Recently, Tsui & Wang (2008) confirmed the findings of Chiang *et al.* (2000), and noted that for $\Lambda \geqslant 24$ the flow structure can be regarded as two-dimensional as the side-wall effects are negligible in the central part of the channel. In addition to the symmetry breaking of the two-dimensional flow, the simulations of Chiang *et al.* (2001) revealed the existence of a spanwise modulated three-dimensional flow for certain initial conditions. The flow with spanwise modulation was found to be symmetric with respect to the mid-span plane as well as with respect to the mid-channel plane. Since the corresponding two-dimensional solution, which is symmetric with respect to the mid-channel plane, is unstable, the modulated three-dimensional flow is difficult to obtain numerically and could only be observed for $\Lambda \geqslant 30$.

To date, all linear stability analyses have dealt with the first bifurcation of the primary flow to the stationary secondary flow. No results are available on the stability of the asymmetric two-dimensional secondary flows. Fearn *et al.* (1990) and Battaglia *et al.* (1997) anticipated that the asymmetric solutions would become unstable to

https://doi.org/10.1017/jfm.2012.184 Published online by Cambridge University Press

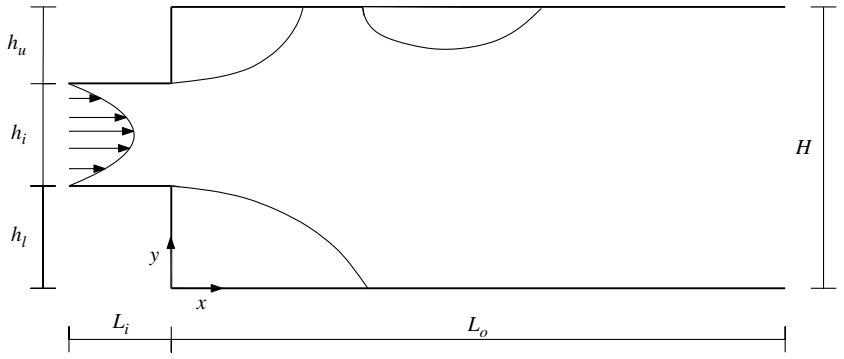


FIGURE 1. Sketch of the channel geometry with a asymmetric sudden expansion and separating streamlines.

three-dimensional perturbations. An alternative was suggested by Cherdron *et al.* (1978) and Durst *et al.* (1993) in which a Hopf bifurcation may result in a time-periodic two-dimensional state. To answer this open question, a three-dimensional global linear stability analysis is carried out in the present work. In doing so the geometry is varied in a quasi-continuous way, covering expansion ratios (step-to-outlet height ratios) from 0.25 to 0.95. It is shown that, within this parameter range, the primary instability of the symmetric basic flow is two-dimensional. Moreover, the asymmetric two-dimensional solutions become unstable to three-dimensional and not to two-dimensional perturbations. In case of an asymmetric geometry the disconnected saddle-node bifurcation point for the disconnected steady two-dimensional solution branches is shifted to higher Reynolds numbers as the channel asymmetry is increased (see figure 4). Hence, even for a slight asymmetry, only the non-symmetric solution of the contiguous branch is relevant for the three-dimensional stability analysis. Its stability boundaries are found to be similar to those of the asymmetric solutions for the symmetric channel flow.

The outline of this paper is as follows. Section 2 deals with the methods of investigation, where the problem is formulated, the governing equations are presented and the numerical code is verified. In § 3, the main part of this work, parameter independence of the critical data is established and the results of the stability calculations are analysed, followed by a detailed discussion of the physical nature of the instabilities. The conclusion in § 4 sums up our main findings.

2. Methods of investigation

2.1. *Problem definition*

We consider an incompressible, Newtonian fluid in a plane channel with a sudden expansion. The system is considered to be infinitely extended in the spanwise (z) direction. The geometry is sketched in figure 1, consisting of an inlet channel of length L_i and height h_i, followed by a suddenly expanded channel of height H and length L_o. The lower step height is denoted by h_l and the upper one by h_u. The origin of the Cartesian coordinate system is located at the bottom of the outlet channel and at the sudden expansion. The geometry is characterized by the expansion ratio

$$\Gamma = \frac{h_l + h_u}{H} = 1 - \frac{h_i}{H} \tag{2.1}$$

https://doi.org/10.1017/jfm.2012.184 Published online by Cambridge University Press

and the asymmetry ratio

$$\alpha = \frac{|h_l - h_u|}{h_s}, \tag{2.2}$$

where $h_s = (h_l + h_u)/2$ denotes the step height for the symmetric case.

The steady flow of an incompressible viscous fluid is governed by the Navier–Stokes and continuity equations

$$\boldsymbol{u}_0 \cdot \boldsymbol{\nabla} \boldsymbol{u}_0 = -\boldsymbol{\nabla} p_0 + \frac{1}{Re} \nabla^2 \boldsymbol{u}_0, \tag{2.3a}$$

$$\boldsymbol{\nabla} \cdot \boldsymbol{u}_0 = 0, \tag{2.3b}$$

where length, velocity and pressure have been made dimensionless with respect to L, U_∞ and ρU_∞^2. To conform with previous investigations and for computational economy, it is useful to define the Reynolds number as

$$Re = \frac{L U_\infty}{\nu}. \tag{2.4}$$

It is based on half of the downstream channel height $L = H/2$ and the maximum (centreline) velocity U_∞ of the inlet profile.

No-slip and no-penetration boundary conditions $\boldsymbol{u}_0 = 0$ are imposed at the channel walls. At the inlet a fully developed laminar plane Poiseuille flow $u_0(y) = 4(y - h_l)(h_i - y + h_l)/h_i^2$ and $v_0 = 0$ is assumed for $y = h_i$. At the outflow boundary the normal derivatives of all velocity components are set to zero, i.e. $\partial_x \boldsymbol{u}_0 = 0$, and the pressure is specified as $p_0 = 0$.

Assuming that the inlet L_i as well as the outlet channel lengths L_o are sufficiently large such that the results are independent of L_i and L_o, the problem is governed by three parameters: the Reynolds number Re (2.4), the expansion ratio Γ (2.1) and the asymmetry α (2.2) of the geometry. The dependence of the stability boundaries on the channel lengths will be considered in more detail in § 3.1.

2.2. *Linear stability analysis*

The global, temporal linear stability of the two-dimensional basic flow $\boldsymbol{u}_0 = (u_0, v_0, 0)^{\mathrm{T}}$ is governed by

$$\partial_t \tilde{\boldsymbol{u}} + \boldsymbol{u}_0 \cdot \boldsymbol{\nabla} \tilde{\boldsymbol{u}} + \tilde{\boldsymbol{u}} \cdot \boldsymbol{\nabla} \boldsymbol{u}_0 = -\boldsymbol{\nabla} \tilde{p} + \frac{1}{Re} \nabla^2 \tilde{\boldsymbol{u}}, \tag{2.5a}$$

$$\boldsymbol{\nabla} \cdot \tilde{\boldsymbol{u}} = 0. \tag{2.5b}$$

The three-dimensional perturbations $\tilde{\boldsymbol{u}} = (\tilde{u}, \tilde{v}, \tilde{w})^{\mathrm{T}}$ and $\tilde{p}$ represent infinitesimal deviations from the basic flow and satisfy the following boundary conditions

$$\tilde{\boldsymbol{u}} = 0 \quad \text{at the inlet and walls,} \tag{2.6a}$$

$$\partial_x \tilde{\boldsymbol{u}} = 0, \quad \tilde{p} = 0 \quad \text{at the outlet.} \tag{2.6b}$$

Hence the total flow $\boldsymbol{u}_0 + \tilde{\boldsymbol{u}}$ satisfies the same boundary conditions as the basic flow $\boldsymbol{u}_0$.

Since the coefficients of (2.5) do not depend on z and t, the general solution can be written as a superposition of normal modes

$$\begin{pmatrix} \tilde{\boldsymbol{u}} \\ \tilde{p} \end{pmatrix} (x, y, z, t) = \begin{pmatrix} \hat{\boldsymbol{u}} \\ \hat{p} \end{pmatrix} (x, y)\, \mathrm{e}^{-\gamma t + \mathrm{i} k z} + \text{c.c.}, \tag{2.7}$$

https://doi.org/10.1017/jfm.2012.184 Published online by Cambridge University Press

where the complex conjugate (c.c.) renders the perturbations real. Here, $k \in \mathbb{R}$ is a real, positive wavenumber in the spanwise direction. The temporal decay rate $\gamma = \sigma + \mathrm{i}\omega \in \mathbb{C}$ of (2.7) comprises the real decay rate $\sigma \in \mathbb{R}$ and the oscillation frequency $\omega \in \mathbb{R}$. Here $\hat{\boldsymbol{u}}$ and $\hat{p}$ represent the complex amplitude/shape functions of the perturbations, which are normalized by setting the maximum norm to 1,

$$\|\hat{\boldsymbol{u}}\|_\infty := \max_{x,y\in\mathscr{D}} \left\{|\hat{u}|, |\hat{v}|, |\hat{w}|\right\} = 1, \tag{2.8}$$

over the computational domain $\mathscr{D}$.

The critical Reynolds number Re_c is characterized by the condition that the minimum possible real decay rate σ vanishes. Consequently the decay rate σ must be minimized over all discrete eigenvectors $\hat{\boldsymbol{x}} = (\hat{\boldsymbol{u}}, \hat{p})^{\mathrm{T}}$ and all continuous wavenumbers k for a certain Reynolds number Re and geometry (Γ, α). The optimization problem can be formulated by

$$\sigma_{min} = \min_{k\in\mathbb{R}} \sigma(k, Re, \hat{\boldsymbol{x}}, \Gamma, \alpha), \tag{2.9}$$

which evaluates to zero for Re_c and k_c.

2.3. *Energy analysis*

The transfer rates of the kinetic energy between the basic state and the critical perturbation flow provide insight into the physical instability mechanism. The kinetic energy per unit mass of the perturbation flow is defined as $E_{kin} = \int_V \tilde{\boldsymbol{u}}^2 \,\mathrm{d}V/2$, where the integration is carried out over the volume $V = [0, 2\pi/k] \times \mathscr{D}$ covering a spanwise period $2\pi/k$ of the perturbations times the computational domain $\mathscr{D}$. Scalar multiplication of the linear perturbation equations (2.5) by $\tilde{\boldsymbol{u}}$ from the left-hand side and integrating over the volume yields the Reynolds–Orr equation, which can be solved for the rate of change of the kinetic energy $\mathrm{d}E_{kin}/\mathrm{d}t$ (see e.g. Kuhlmann 1999) to obtain

$$\frac{1}{D}\frac{\mathrm{d}E_{kin}}{\mathrm{d}t} = -1 + \sum_{i=1}^{4} \int_V I_i' \,\mathrm{d}V - \frac{1}{2}\int_{S_o} I_5 \,\mathrm{d}S. \tag{2.10}$$

The above equation has been normalized by the total dissipation rate

$$D = \frac{1}{Re}\int_V \tilde{\boldsymbol{u}} \cdot \nabla^2 \tilde{\boldsymbol{u}} \,\mathrm{d}V. \tag{2.11}$$

The surface integral at the outlet,

$$-\frac{1}{2}\int_{S_o} I_5 \,\mathrm{d}S = -\frac{1}{2}\int_{S_o} \frac{\tilde{\boldsymbol{u}}^2 u_0}{D} \,\mathrm{d}S, \tag{2.12}$$

describes the transfer rate of the kinetic perturbation energy which is advected out of the domain by the basic flow. Pressure forces do not contribute to the energy budget, as we assume a constant pressure perturbation $\tilde{p}$ at the outlet. In addition, no perturbation energy is convected into the domain, either through the inlet or through the solid walls on which $\tilde{\boldsymbol{u}} = 0$.

For an analysis of the energy transfer rates it is useful to decompose the perturbation velocity $\tilde{\boldsymbol{u}}$ into components parallel ($\tilde{\boldsymbol{u}}_\parallel$) and perpendicular ($\tilde{\boldsymbol{u}}_\perp$) to the basic flow $\boldsymbol{u}_0$,

$$\tilde{\boldsymbol{u}}_\parallel = \frac{(\tilde{\boldsymbol{u}} \cdot \boldsymbol{u}_0)\boldsymbol{u}_0}{\boldsymbol{u}_0 \cdot \boldsymbol{u}_0}, \quad \tilde{\boldsymbol{u}}_\perp = \tilde{\boldsymbol{u}} - \tilde{\boldsymbol{u}}_\parallel, \tag{2.13}$$

https://doi.org/10.1017/jfm.2012.184 Published online by Cambridge University Press

such that the local normalized energy transfer terms are given by

$$\sum_{i=1}^{4} I_i' = -\frac{1}{D}\left[\tilde{\boldsymbol{u}}_\perp \cdot (\tilde{\boldsymbol{u}}_\perp \cdot \nabla \boldsymbol{u}_0) + \tilde{\boldsymbol{u}}_\parallel \cdot (\tilde{\boldsymbol{u}}_\perp \cdot \nabla \boldsymbol{u}_0) + \tilde{\boldsymbol{u}}_\perp \cdot (\tilde{\boldsymbol{u}}_\parallel \cdot \nabla \boldsymbol{u}_0) + \tilde{\boldsymbol{u}}_\parallel \cdot (\tilde{\boldsymbol{u}}_\parallel \cdot \nabla \boldsymbol{u}_0)\right]. \tag{2.14}$$

Each term represents a certain energy transport process. The use of the coordinates, locally aligned with the flow direction $\boldsymbol{u}_0/u_0$, is suitable, because no other distinguished direction exists locally. As an example, I_2' is the local rate of change of perturbation energy density per unit mass by the convective transport due to a cross-stream perturbation flow $(\tilde{\boldsymbol{u}}_\perp \cdot \nabla)$ of basic-state momentum $(\boldsymbol{u}_0)$. Hence, if $\tilde{\boldsymbol{u}}_\perp \cdot \nabla \boldsymbol{u}_0$ has a component parallel to and in the direction of $\tilde{\boldsymbol{u}}_\parallel$, kinetic energy is locally transferred from the basic state to the perturbation flow. If $I_2' < 0$, the perturbation locally loses energy to the basic flow. Note that the energy budget also serves as a verification for the linear stability results, since the rate of change of the kinetic energy has to vanish for the critical mode, i.e.

$$\left.\frac{\mathrm{d}E_{kin}}{\mathrm{d}t}\right|_{\sigma=0} = 0. \tag{2.15}$$

2.4. *Numerical methods and code verification*

The numerical methodology is the same as that of Lanzerstorfer & Kuhlmann (2012*a*), where details and references can be found. In brief, a finite-volume discretization of second order is employed, in which the primitive variables are discretized on a staggered grid. The grid is refined geometrically near the walls and around the step, such that neighbouring cells do not differ by more than 3 % in width. The nonlinear system (2.3) for the basic state is solved by the Newton–Raphson method.

The complex, generalized and singular eigenvalue problem originating from the linear stability analysis is transformed into a real-valued problem to save computational time and memory. Two spectral transformations are made: in a first step, a shift-invert transformation with zero shift is carried out in order to find the eigenvalues with smallest magnitude. Thereafter, a Cayley transformation is used which guarantees that the eigenvalues with smallest real part are detected. All eigenvalue problems are solved with an implicitly restarted Arnoldi algorithm using a Krylov subspace dimension of 80 (Lehoucq & Sorensen 1996). The results have been checked using a Krylov subspace dimension of 150 and 250 which, however, did not yield different results. A higher Krylov subspace dimension should guarantee that no dangerous, especially critical, eigenvalue is missed in the approximation of the spectrum.

The results were found to be grid-independent if the grid resolution is at least $\Delta x_{min} = \Delta y_{min} = 0.005$ (in units of L) along the walls and around the step. For generating the various grids, Δx_{min} and Δy_{min} are specified at the walls. Then the cell width is increased towards the bulk using a constant stretching factor of 1.03 until the predefined maximum grid spacings of $\Delta x_{max} = 0.075$ and $\Delta y_{max} = 0.025$, respectively, are reached. The maximum cell size is then kept constant up to the boundaries of the geometry. This meshing strategy maintains a relatively constant cell density across the inflow channel. Relevant grid parameters for representative expansion ratios can be found in table 4 in the Appendix.

https://doi.org/10.1017/jfm.2012.184 Published online by Cambridge University Press

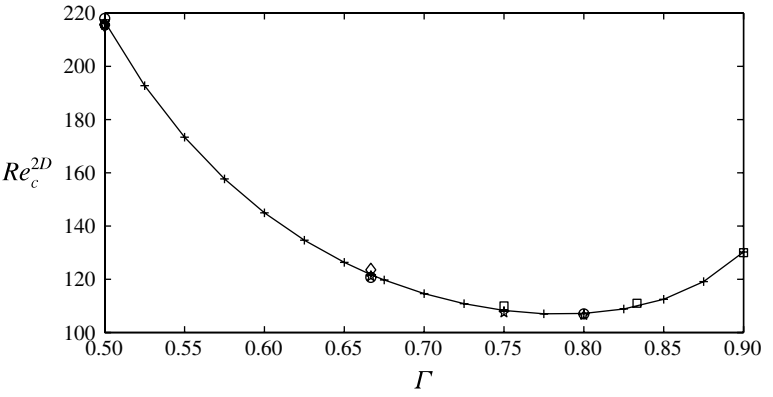


FIGURE 2. Critical Reynolds number for the two-dimensional instability of the symmetric flow for $\alpha = 0$ (line and plus signs) as function of the expansion ratio Γ with $L_o = 25L$. Also shown are the results of Shapira & Degani (1990) (diamonds), Alleborn *et al.* (1997) (circles), Battaglia *et al.* (1997) (stars) and Drikakis (1997) (squares).

The numerical code was verified thoroughly in Lanzerstorfer & Kuhlmann (2012*a*,*b*) by checking the results against those found in the literature for several systems, such as plane-channel flow, lid-driven square cavity, backward-facing-step and forward-facing-step problems. To give further credence to the present numerical code, the two-dimensional stability boundaries for the symmetric solution are compared with those obtained by Shapira & Degani (1990), Alleborn *et al.* (1997), Battaglia *et al.* (1997) and Drikakis (1997). The result is depicted in figure 2. The data, computed with an outflow-channel length of $L_o = 25L$, are consistent and show a very good agreement.

3. Results and discussion

3.1. *Dependence on channel lengths*

The influence of the entrance length L_i and the length of the outflow channel L_o on the stability boundaries was analysed in order to ensure that the critical data are independent of these two geometry parameters. Different critical Reynolds numbers arise. For clarity, the critical Reynolds numbers (as well as wavenumbers) for the two-dimensional instability of the symmetric two-dimensional basic flow in the symmetric geometry (primary instability for $\alpha = 0$) will be denoted by Re_c^{2D}, the three-dimensional critical Reynolds number of the asymmetric two-dimensional basic flow in the symmetric geometry (secondary instability for $\alpha = 0$) is denoted by Re_c^0, and the critical Reynolds number for the continuous two-dimensional basic flow in the perturbed (asymmetric, $\alpha \neq 0$) geometry is called Re_c^α.

The effect of the inlet channel length L_i on the stability boundaries is shown in table 1. Results are reported for $\Gamma = 0.5$ for the asymmetric solution of the symmetric channel Re_c^0, but a similar convergence of the critical data, as L_i is increased, holds true for all expansion ratios covered here, and also for the asymmetric channel geometry. As can be observed from table 1, the entrance length should be at least $L_i = 6h_i$. In the current study the inlet channel length was set to $L_i = 8h_i$ to keep its effect on the critical data below $\approx 0.02\,\%$. Such a long entrance length is necessary

https://doi.org/10.1017/jfm.2012.184 Published online by Cambridge University Press

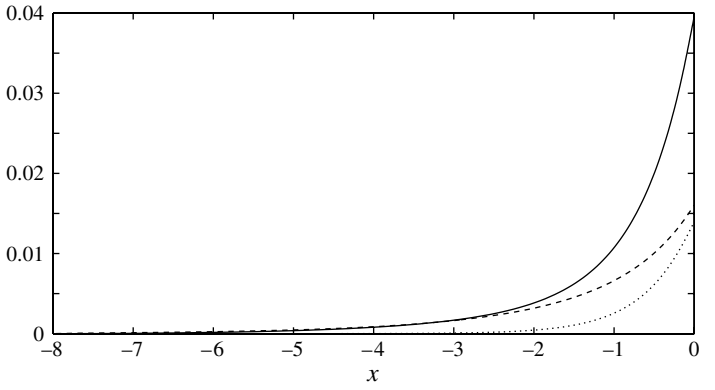


FIGURE 3. Maxima of the velocity-perturbation components in the inlet channel for $\Gamma = 0.5$ at $Re_c^0 = 790.94$ and $k_c^0 = 0.6317$. The solid, dotted and dashed lines represent $\max_y |\hat{u}(x, y)|$, $\max_y |\hat{v}(x, y)|$ and $\max_y |\hat{w}(x, y)|$, respectively, in units of (2.8).

L_i	$1h_i$	$2h_i$	$3h_i$	$4h_i$	$6h_i$	$8h_i$	$15h_i$
Re_c^0	806.47	797.17	793.25	791.63	790.98	790.94	790.94
k_c^0	0.6615	0.6490	0.6387	0.6340	0.6318	0.6317	0.6317

TABLE 1. Critical values Re_c^0 and k_c^0 as functions of the entrance length L_i for multiples of the inlet channel height h_i for $\Gamma = 0.5$ with $L_o = 65$.

because the critical mode extends well upstream of the expansion, which is shown in figure 3.

The influence of the outflow length L_o on the results was also investigated. The required outflow channel length L_o depends on the Reynolds number (see the Appendix). It must be long enough for a plane Poiseuille flow to be developed at the outlet. The outlet length is selected such that the maximum relative deviation of the x-component of the outlet velocity profile from a plane Poiseuille flow is less than 2 %. Note that if L_o is too short, unphysical modes may arise for high Krylov subspace dimensions ($\geqslant$150), being artefacts of the outlet boundary conditions.

3.2. *Stability boundaries*

Since the basic two-dimensional flow beyond the primary instability threshold Re_c^{2D} is not unique, care must be taken to find the symmetric and asymmetric basic flows by Newton iteration. To stay on the basic symmetric-flow solution branch for $\alpha = 0$ and $Re > Re_c^{2D}$ it suffices to increase the Reynolds number stepwise by less than 10 % using the previously computed solution as the initial guess. To find and track one of the two asymmetric solutions we used $u_0 \equiv v_0 \equiv 1$ and $p_0 \equiv 0$ as the initial guess for the Newton iteration, and the Reynolds number is selected as $Re > 1.2 \times Re_c^{2D}$, using the same step size in Re as for the symmetric-solution tracking.

Figure 4 shows for $\Gamma = 0.\dot{6}$ the topological change of the pitchfork bifurcation diagram upon an asymmetric geometry perturbation as described in the Introduction.

https://doi.org/10.1017/jfm.2012.184 Published online by Cambridge University Press

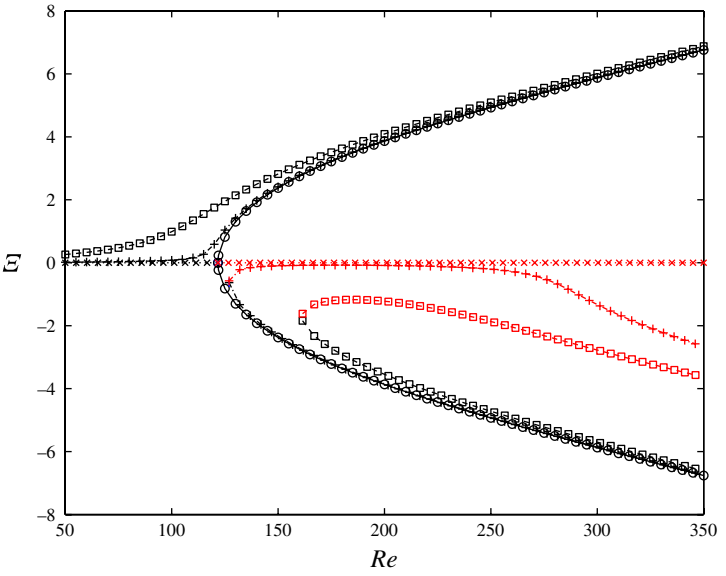


FIGURE 4. (Colour online available at journals.cambridge.org/flm) The measure of asymmetry (3.1) for various basic-flow solutions. Crosses and dots represent the symmetric flow, and circles and solid lines indicate the asymmetric flow solutions for the symmetric channel $\alpha = 0$. Plus signs and dash-dotted lines denote the flow solutions of the slightly asymmetric geometry $\alpha = 0.01$, whereas squares and dashed lines represent those for $\alpha = 0.15$.

The following measure of asymmetry is chosen to be

$$\Xi = \mathrm{sgn}(x_l - x_u)\sqrt{\int (\partial_y u_0|_{y=H} + \partial_y u_0|_{y=0})^2 \, \mathrm{d}x}, \tag{3.1}$$

where x_l and x_u denote the lengths of the lower and the upper primary recirculation bubbles, respectively, and the wall shear stresses are evaluated at the upper and lower walls of the outlet channel. For a symmetric geometry ($\alpha = 0$) the basic symmetric-flow solution, depicted by crosses and dots, becomes unstable at $Re_c^{2D} = 121.74$. At this critical Reynolds number two stable and asymmetric flow solutions (circles and solid lines) bifurcate via a perfect pitchfork bifurcation. If the expansion is slightly asymmetric ($\alpha \neq 0$), the bifurcation becomes imperfect (plus signs and dash-dotted lines) and a saddle-node bifurcation arises at $Re^{SN}(\alpha = 0.01) \approx 127$. The disconnected saddle-node bifurcation point is shifted to higher Reynolds numbers as the channel asymmetry is increased. This is shown for $\alpha = 0.15$ by squares and dashed lines, where the saddle-node bifurcation point is located at $Re^{SN}(\alpha = 0.15) \approx 161.5$. In this case, the connected solution branch deviates substantially from the flow solutions corresponding to $\alpha = 0$ in the vicinity of $Re_c^{2D} = 121.74$. However, the differences are getting smaller as the Reynolds number is increased. The upper solution branch emerging from the saddle-node bifurcation point is unstable from the beginning, which is indicated in grey (red online). The substantial deviation of Ξ from zero for the unstable supercritical solution for $\alpha = 0.01$ at Reynolds numbers $Re \approx> 250$ is due to the creation of a third recirculation bubble.

https://doi.org/10.1017/jfm.2012.184 Published online by Cambridge University Press

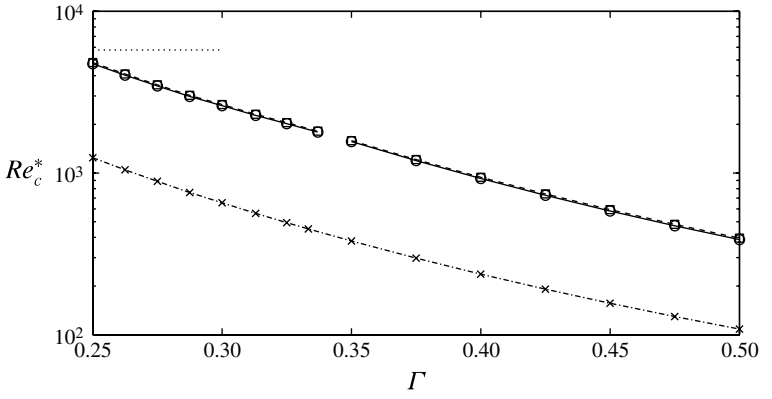


FIGURE 5. Scaled critical inlet Reynolds numbers as functions of the expansion ratio Γ. Crosses and the dash-dotted line represent Re_c^{2D*}, open circles and the solid line indicate Re_c^{0*}, and open squares and the dashed line represent $Re_c^{\alpha*}$ for $\alpha = 0.15$. The dotted line indicates the critical Reynolds number of plane Poiseuille flow. All Reynolds numbers are shown on a logarithmic scale.

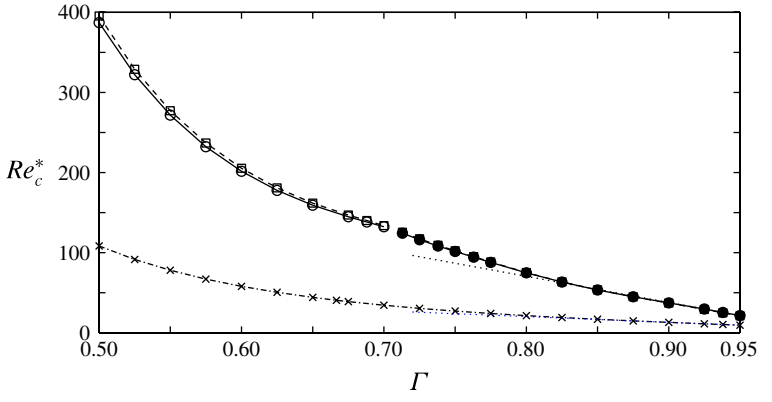


FIGURE 6. Scaled critical inlet Reynolds numbers as functions of the expansion ratio Γ. Crosses and the dash-dotted line represent Re_c^{2D*}, circles and the solid line indicate Re_c^{0*}, and squares and the dashed line represent $Re_c^{\alpha*}$ for $\alpha = 0.15$. Open symbols stand for stationary modes, solid ones for oscillatory modes. The dotted lines indicate the linear behaviour for $\Gamma \to 1$ as mentioned in the text.

In the present study we restrict our attention to the connected solution branch with $\alpha = 0.15$ (squares and dashed lines in figure 4). In fact, the stability boundaries for $\alpha = 0.15$ are very similar to the critical data of the corresponding asymmetric solution for $\alpha = 0$, i.e. for the symmetric geometry (see figures 5 and 6).

Representative numerical critical Reynolds numbers, wavenumbers and oscillation frequencies can be found in table 4 in the Appendix. Data are provided for selected expansion ratios for the primary instability (Re_c^{2D}) and the secondary instability (Re_c^0), both in the symmetric channel and also for the instability of the asymmetric flow of the connected solution branch (Re_c^α) in the asymmetric geometry ($\alpha = 0.15$). Moreover, the outflow lengths L_o and the number of grid points are specified.

https://doi.org/10.1017/jfm.2012.184 Published online by Cambridge University Press

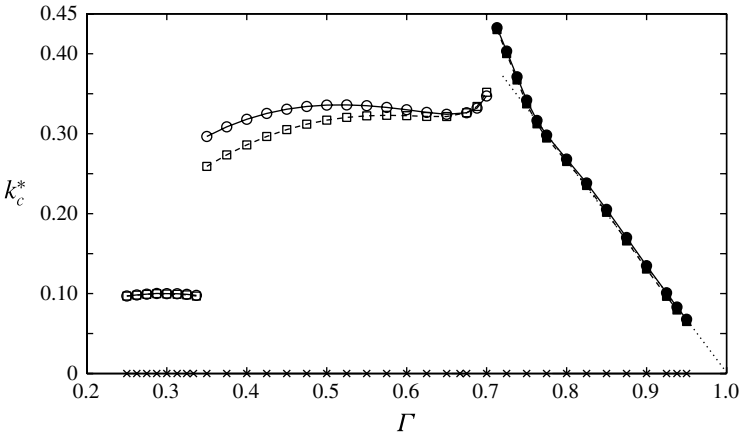


FIGURE 7. Scaled critical wavenumbers k_c^* as functions of the expansion ratio Γ. Crosses represent k_c^{2D*}, circles and the solid line indicate k_c^{0*}, and squares and the dashed line $k_c^{\alpha*}$ for $\alpha = 0.15$. Open symbols stand for stationary modes, solid ones for oscillatory modes. The dotted line indicates the linear behaviour as mentioned in the text.

For an overview of the critical data these are rescaled here in the § 3.2 using the inlet velocity U_∞ and inlet length scale $h_i/2$, and we define

$$Re^* = Re\frac{h_i}{H}, \quad k^* = k\frac{h_i}{H}, \quad \omega^* = \omega\frac{h_i}{H}. \tag{3.2}$$

The inlet Reynolds number $Re^* = U_\infty^{inlet} h_i/2\nu = U_\infty^{outlet} H/2\nu$ is equivalent to the one at the outlet.

Figure 5 shows various critical inlet Reynolds numbers (Re_c^{2D*}, Re_c^{0*} and $Re_c^{\alpha*}$, respectively) on a logarithmic scale as functions of the expansion ratio for $\Gamma \leqslant 0.5$. In the range shown, all critical modes are stationary and the stability boundaries scale nearly exponentially with Γ. The stability boundaries of the asymmetric flow in the symmetric channel Re_c^{0*} are very similar to those of the solution in the asymmetric channel $Re_c^{\alpha*}$ for $\alpha = 0.15$, which can be seen by the two overlapping curves in figures 5 and 6. Note that the gap between the curves at $\Gamma \in [0.337; 0.35]$ should indicate that the critical modes and their underlying instability mechanisms change (see also figure 7). Moreover, the critical Reynolds number for the symmetric flow Re_c^{2D*} is smaller than Re_c^{0*} and $Re_c^{\alpha*}$ by approximately a factor of 1/4. Even for the smallest step height considered, i.e. $\Gamma = 0.25$, all critical Reynolds numbers are below the linear stability boundary $Re_c^{Poiseuille} = 5772$ of plane Poiseuille flow, which is indicated by a dotted line in figure 5.

As the step height is increased, the critical inlet Reynolds number decreases continuously and scales linearly for very large expansion ratios $(1 - \Gamma) \ll 1$, as shown in figure 6. The linear asymptotic behaviour for $(1 - \Gamma) \ll 1$ is estimated as $Re_c^{2D*} \approx 77.60 - 71.75 \times \Gamma$ and $Re_c^{0*} \approx Re_c^{\alpha*} \approx 331.64 - 326.43 \times \Gamma$, respectively. As can be seen from figure 6, the difference in the critical Reynolds numbers between the symmetric (Re_c^{2D*}) and asymmetric solutions (Re_c^{0*} and $Re_c^{\alpha*}$) decreases continuously (also relatively) as Γ is increased.

We find that the critical modes corresponding to Re_c^{0*} and $Re_c^{\alpha*}$ change twice in the range of expansion ratios considered. Since the slopes of the intersecting neutral curves are nearly the same, the modal change is more easily seen in the jump

https://doi.org/10.1017/jfm.2012.184 Published online by Cambridge University Press

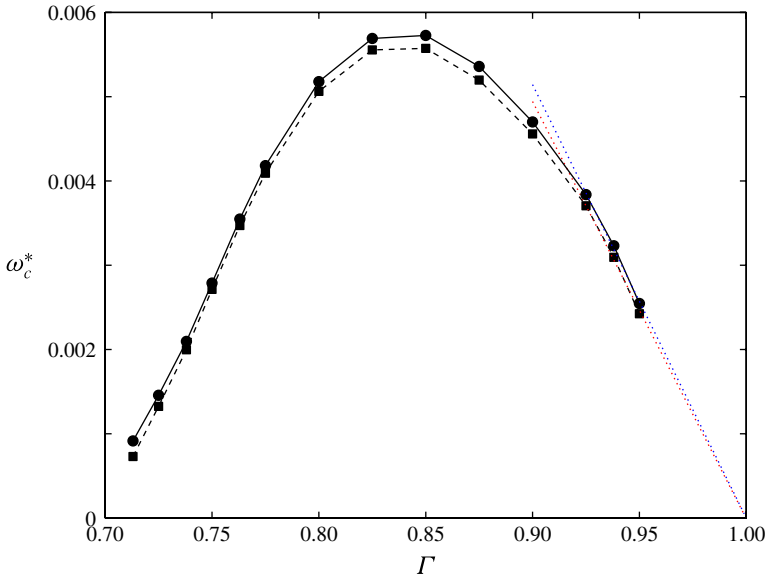


FIGURE 8. (Colour online) Scaled critical frequencies ω_c^* as functions of the expansion ratio Γ. Circles and the solid line represent ω_c^{0*}, squares and the dashed line $\omega_c^{\alpha*}$ for $\alpha = 0.15$. The dotted lines indicate the asymptotes for $\Gamma \to 1$ as mentioned in the text.

of the critical wavenumbers, shown in figure 7. The first modal change is among stationary modes and it arises in the interval $\Gamma \in [0.337; 0.35]$. The second modal change is from a steady to an oscillatory mode and occurs within $\Gamma \in [0.7; 0.713]$. From figure 7 it is also observable that the two wavenumbers k_c^{0*} and $k_c^{\alpha*}$ remain approximately constant ($\approx$0.1) for small step heights and scale linearly for large expansion ratios, which is estimated as $k_c^{0*} \approx k_c^{\alpha*} \approx 1.33 - 1.32 \times \Gamma$. The scaled frequencies ω_c^* of the critical modes are shown in figure 8 for large expansion ratios $\Gamma > 0.7$. The asymptotes are estimated by $\omega_c^{0*} \approx 0.05 \times (1 - \Gamma)$ (less steep dotted line, red online) and $\omega_c^{\alpha*} \approx 0.051 \times (1 - \Gamma)$ (steeper dotted line, blue online), respectively.

Regardless of the expansion ratio Γ, the two-dimensional basic flow immediately behind the expansion is characterized by two separated recirculation zones which are symmetric for $\alpha = 0$ and $Re \leqslant Re_c^{2D}$. They are referred to as primary vortices. For the asymmetric basic flows at higher Reynolds numbers, three recirculation bubbles are present. Two of them separate immediately downstream of the sharp corners. The stronger and larger of theses vortices will be called primary, the weaker and smaller vortex on the opposite side of the channel the secondary vortex. On the same side of the weaker vortex further downstream, a third separated vortex arises. Even though the computational domain is much more extended in the streamwise (x) direction, we shall discuss only the flow characteristics near the separated vortices, because these regions are found to be of key importance for the flow instabilities. It is these regions where the critical modes and the associated energy transfer rates are most pronounced.

3.3. *Symmetry-breaking bifurcation in the symmetric expansion*

The physical nature of the two-dimensional instability of the primary, symmetric flow for $\alpha = 0$ is nearly independent of the expansion ratio. As a representative case for a strong expansion, the primary, symmetry-breaking instability for $\Gamma = 0.9$ is considered.

https://doi.org/10.1017/jfm.2012.184 Published online by Cambridge University Press

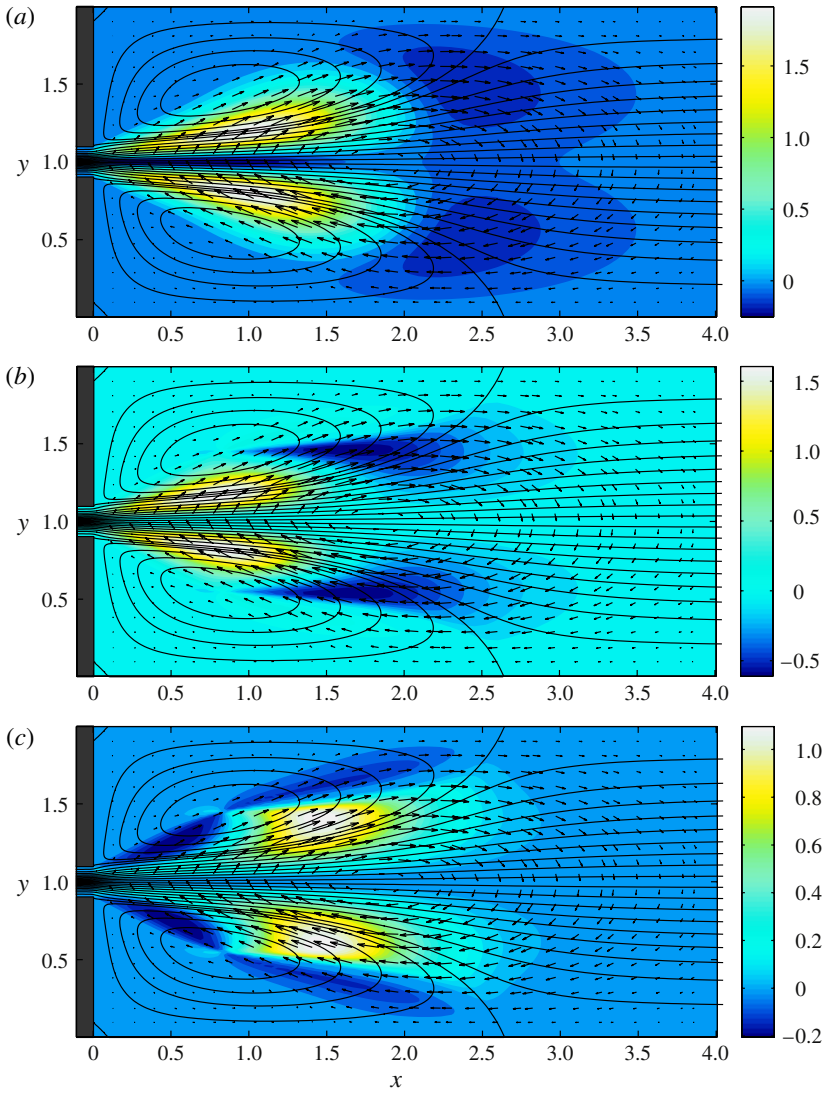


FIGURE 9. (Colour online) Basic state streamlines, critical velocity fields (arrows) and local energy production rates for $\Gamma = 0.9$ and $Re_c^{2D} = 130.17$. (*a*) Total local production $\sum_i I_i'$, (*b*) I_2', and (*c*) I_4'.

The critical Reynolds number is $Re_c^{2D} = 130.17$. As can be seen from figure 9, the basic flow is symmetric and represents a jet into a laterally bounded domain. The counter-rotating recirculation zones are approximately three times as long as the step height. The critical mode appears as a single vortex centred at the axis of symmetry $y = 1$ and spanning the full width of the outlet channel.

From figure 9(*a*) it can be noticed that most of the kinetic energy is transferred from the basic state to the perturbations in the shear layers near the separating streamlines. The total local energy transfer peaks at around $x \approx 1$. The largest integral contribution to the energy transfer is due to I_4' (see table 2), which describes the streamwise transport of basic flow momentum $\tilde{\boldsymbol{u}}_{\parallel} \cdot \boldsymbol{\nabla} \boldsymbol{u}_0$, feeding back on the streamwise

https://doi.org/10.1017/jfm.2012.184 Published online by Cambridge University Press

i	1	2	3	4	Γ
$\int_{\mathscr{D}} I_i' \,\mathrm{d}\mathscr{D}$	−0.1480	0.3577	0.0316	0.7587	0.9
$\int_{\mathscr{D}} I_i'^{+} \,\mathrm{d}\mathscr{D}$	0.0355	0.4322	0.0625	0.4699	0.9
$\int_{\mathscr{D}} I_i' \,\mathrm{d}\mathscr{D}$	−0.0474	−0.1418	0.0441	1.1451	0.25
$\int_{\mathscr{D}} I_i'^{+} \,\mathrm{d}\mathscr{D}$	0.0149	0.8057	0.0067	0.1727	0.25

TABLE 2. Global normalized energy production rates for the symmetry-breaking bifurcation. $\int_{S_o} I_5 \,\mathrm{d}S = 0$ for all cases considered.

perturbation flow $\tilde{\boldsymbol{u}}_{\parallel}$. In order for this process to have a destabilizing effect, the basic flow must decelerate, i.e. $\boldsymbol{e}_{\parallel} \cdot \boldsymbol{\nabla} \boldsymbol{u}_0 < 0$. The term I_4' is most pronounced within the separation zones with maximum energy production near $x \approx 1.5$. Its importance, however, is quantified, because the process I_2' is locally stabilizing in the same region (see figure 9*b,c*). The term I_2' exhibits the strongest local maxima, which are reflected in the total local production (figure 9*a*). The amplification process I_2' requires a high shear rate, which is present in the shear layers between the separation zones and the bulk flow.

Table 2 shows the global normalized energy production rates for the symmetry-breaking bifurcation. The integrals are also evaluated over the flow domain $\mathscr{D}$ restricted to positive values of the integrands $I_i'^{+}$. This yields their relative contribution to the destabilizing energy transfer. It can be noticed that the terms $I_2'^{+}$ and $I_4'^{+}$ are indeed of comparable importance. We thus argue that the two-dimensional symmetry-breaking instability at $\Gamma = 0.9$ is based on the combined effects of flow deceleration and shear-layer instability.

It is worth mentioning that Shtern & Hussain (2003) found similar instabilities for conical jets. They showed via a non-parallel analysis that flow deceleration plays a major role for swirl-free jets, triggering non-axisymmetric instabilities.

When the step height is decreased, the primary vortices become very much elongated downstream. For $\Gamma = 0.25$, for instance, the recirculating zones are approximately 34 times as long as the step height and the bulk flow is almost parallel (see figure 10). Again, the critical mode arises as a single stationary vortex centred at the line of symmetry, but this vortex is much more elongated than in the case of $\Gamma = 0.9$.

As can be seen from table 2, the term $I_2'^{+}$ is clearly dominating and $I_4'^{+}$ plays only a subordinate role. For that reason the total local energy production $\sum_i I_i'$ is qualitatively the same as I_2'. The former is displayed in figure 10. Therefore, the symmetric basic flow becomes unstable for $\Gamma = 0.25$ due to the high shear between the recirculating bubbles and the almost parallel jet in the bulk. The two-dimensional nature of the instability for this nearly parallel flow is consistent with Squire's theorem (Squire 1933). Moreover, the velocity profile of the basic flow has a turning point, consistent with Rayleigh's theorem for inviscid flows.

https://doi.org/10.1017/jfm.2012.184 Published online by Cambridge University Press

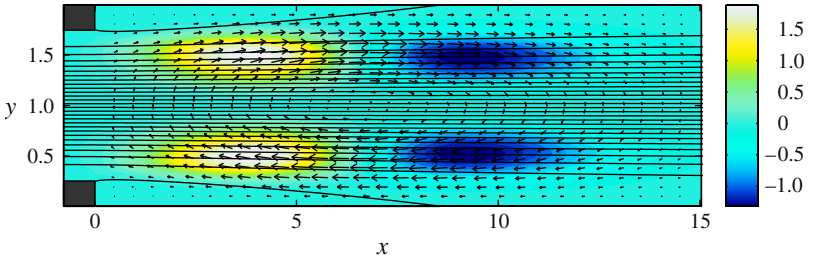


FIGURE 10. (Colour online) Basic state streamlines, critical velocity fields (arrows) and the total local energy production $\sum_i I_i' \approx I_2'$ for $\Gamma = 0.25$ at $Re_c^{2D} = 1657.7$. Note that the scaling of the y-axis is 2.5 times larger than that of x.

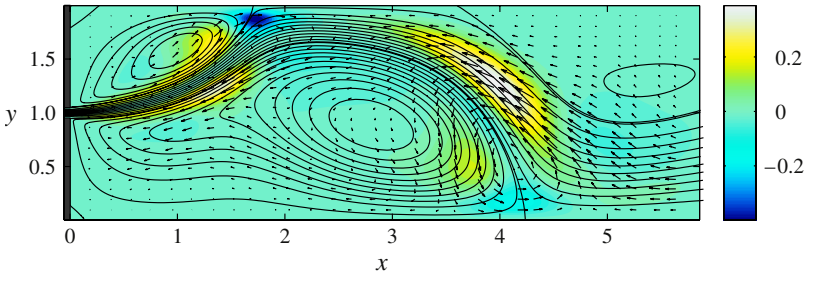


FIGURE 11. (Colour online) Basic state streamlines, critical velocity fields (arrows) and total local energy production $\sum_i I_i'$ for $\Gamma = 0.95$ and $Re_c^0 = 423.48$ at $z = \text{const.}$

3.4. *Three-dimensional oscillatory instability for large expansion ratios* $\Gamma \geqslant 0.713$

In the following we consider the linear stability of the asymmetric two-dimensional basic flow.

3.4.1. *Centrifugal instability for very large expansion ratios*

For very large expansion ratios, the basic state streamlines of the primary eddy are almost circular near its centre and they are only slightly strained. This can be seen in figure 11 for $\Gamma = 0.95$ at critical conditions, i.e. $Re_c^0 = 423.48$ and $k_c^0 = 1.3031$. In this figure the basic flow and the critical mode are shown in a cross-section $z = \text{const.}$, in which the total local energy transfer rate has its global maximum. The local flow is qualitatively the same near the two reattachment points $(x_t, y_t) \approx (1.69, 2)$ and $(x_b, y_b) \approx (4.20, 0)$ of the two separating streamlines, which originate near the sharp edges of the expansion. We also find that the local structure of the critical mode is similar near these points and consists of a vortex each, centred on the separating streamline slightly upstream of the reattachment point. There are also two regions of local energy transfer to the perturbation flow, which are stretched and located on the convex side of the jet, which is formed between the two separating streamlines of the basic flow. The local flow has curved streamlines and the velocity is rapidly decreasing outwards. Such flow conditions are prone to centrifugal effects, and we argue that the instability mechanism is of centrifugal type. This interpretation is supported by the criterion proposed by Sipp & Jacquin (2000), which is a reformulation of Bayly's (1988) sufficient condition for centrifugal instability for two-dimensional, inviscid

https://doi.org/10.1017/jfm.2012.184 Published online by Cambridge University Press

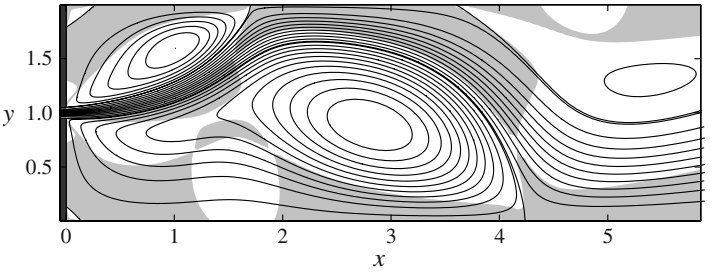


FIGURE 12. Basic state streamlines and grey regions where (3.3) is satisfied for $\Gamma = 0.95$ and $Re_c^0 = 423.48$.

	$\Gamma = 0.25$		$\Gamma = 0.5$		$\Gamma = 0.8$		$\Gamma = 0.95$	
i	$\int_V I_i' \,\mathrm{d}V$	$\int_V I_i'^{+} \,\mathrm{d}V$	$\int_V I_i' \,\mathrm{d}V$	$\int_V I_i'^{+} \,\mathrm{d}V$	$\int_V I_i' \,\mathrm{d}V$	$\int_V I_i'^{+} \,\mathrm{d}V$	$\int_V I_i' \,\mathrm{d}V$	$\int_V I_i'^{+} \,\mathrm{d}V$
1	−0.0518	0.0201	0.0947	0.0997	0.0586	0.1082	−0.0194	0.0981
2	−0.1925	0.8744	0.2843	0.5507	0.6856	0.5452	0.6382	0.4827
3	0.0801	0.0095	0.0545	0.0683	0.0178	0.0957	0.0748	0.1459
4	1.1756	0.0960	0.5752	0.2813	0.2406	0.2626	0.3067	0.2747
$\int_{S_o}$	−0.0114		−0.0087		−0.0002		0.0000	

TABLE 3. Global normalized energy production rates for selected expansion ratios for the asymmetric flow solutions Re_c^0.

flows. Accordingly, the inviscid flow is centrifugally unstable if

$$\frac{|\boldsymbol{u}_0|\zeta}{R} < 0 \tag{3.3}$$

is satisfied all along a closed streamline $\psi = \text{const}$. Here ζ stands for the vorticity of the basic flow and R for the local algebraic radius of curvature, given by

$$R = \frac{|\boldsymbol{u}_0|^3}{(\boldsymbol{\nabla}\psi)\cdot(\boldsymbol{u}_0\cdot\boldsymbol{\nabla}\boldsymbol{u}_0)}. \tag{3.4}$$

Figure 12 shows in grey regions where (3.3) holds true. By comparing figures 11 with 12, it can be observed that total local energy transfer is peaked and stretched parallel to the streamlines in just the grey regions where (3.3) is satisfied.

Moreover, one can hardly notice any difference between $\sum_i I_i'$ and I_2' (not shown), as the term I_2' is the most significant one in the integral sense (table 3). This observation is compatible with the interpretation that the flow becomes centrifugally unstable for very large expansion ratios $(1-\Gamma) \ll 1$.

It is interesting that the wavelength $\lambda_c^0 = 2\pi/k_c$ of the unstable mode does not scale with the thickness of the local shear layer. Instead, the critical mode has a comparatively long wavelength of $\lambda_c^0 = 4.8217$. Moreover, owing to the relatively low critical oscillation frequency $|\omega_c^0| = 0.0485$, the propagating wave travels only slowly in the spanwise direction.

https://doi.org/10.1017/jfm.2012.184 Published online by Cambridge University Press

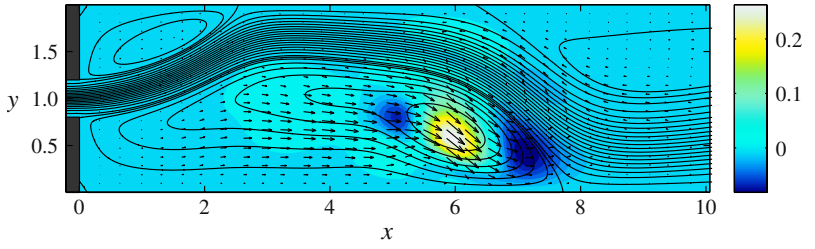


FIGURE 13. (Colour online) Basic state streamlines, critical velocity fields (arrows) and the total local energy production $\sum_i I_i'$ for $\Gamma = 0.8$ and $Re_c^0 = 375.98$ at $z = \text{const}$.

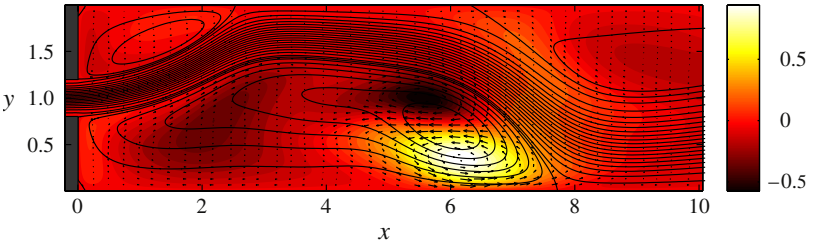


FIGURE 14. (Colour online) Basic state streamlines, vorticity of the critical mode (arrows) and $\tilde{w}$ (intensity) for $\Gamma = 0.8$ and $Re_c^0 = 375.98$ at $z = z_{amp} + \lambda_c^0/4$.

Note that the critical mode and the type of instability are the same as those detected by Lanzerstorfer & Kuhlmann (2012*a*) in the backward-facing-step problem for $\Gamma_{BFS} > 0.9$ because the base flows are locally quite similar.

3.4.2. *Elliptic instability for large expansion ratios*

As the expansion ratio is decreased, the critical mode changes continuously in a progressive manner and the centrifugal instability mechanism is phased out by an elliptic type of instability. The elliptic mechanism becomes dominant at around $\Gamma \lesssim 0.9$ and it also remains operative for smaller expansion ratios down to $\Gamma = 0.713$.

As a representative example, the flow structure is discussed for $\Gamma = 0.8$, where the asymmetric basic flow becomes unstable at $Re_c^0 = 375.98$ with $k_c^0 = 1.3262$. In contrast to very large expansion ratios $(1 - \Gamma) \ll 1$, the primary vortex of the basic flow extends further downstream and undergoes considerable strain (see figure 13). The critical mode is confined within the primary eddy and is strongest in its centre. Figure 13 shows the spanwise plane $z = \text{const.}$, in which the total local energy transfer takes its maximum. In that plane, almost all the kinetic energy is produced in the centre of the elliptic vortex of the basic flow, which is a hallmark of an elliptic instability (Pierrehumbert 1986; Sipp & Jacquin 1998). Figure 14 depicts the spanwise perturbation component $\tilde{w}$ in a plane z_{amp}, in which it has its maximum amplitude. This z_{amp} plane is shifted by a quarter of the critical wavelength $\Delta z = \pi/(2k_c^0)$. Figure 14 also shows the vorticity of the perturbation flow. The vorticity makes an angle of approximately 45° with respect to the major and minor axes of the elliptic streamlines, and is therefore aligned with the principal direction of strain. Such behaviour is another distinctive feature of the critical mode due to an elliptic instability (Waleffe 1990).

https://doi.org/10.1017/jfm.2012.184 Published online by Cambridge University Press

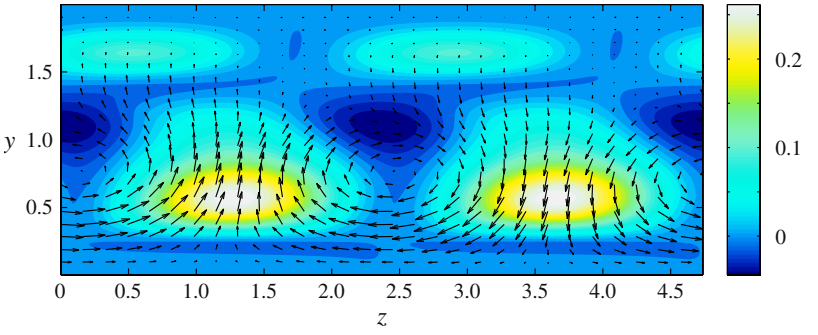


FIGURE 15. (Colour online) Critical perturbation flow (arrows) and total local energy production $\sum_i I_i'$ for $\Gamma = 0.8$ and $Re_c^0 = 375.98$ at $x = 6.0082$. The wave propagates to the right.

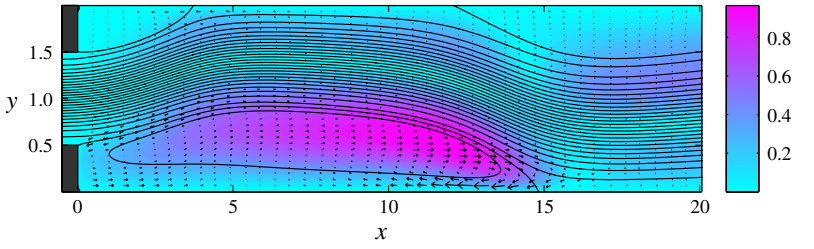


FIGURE 16. (Colour online) Basic state streamlines, spanwise vorticity of the critical mode (arrows) and $|\hat{\boldsymbol{u}}|$ (intensity) for $\Gamma = 0.5$ and $Re_c^0 = 790.95$.

At the margin of stability, the critical flow appears in the form of cellular structures, where the spanwise perturbation component $\tilde{w}$ vanishes periodically on equally spaced planes separated by $\Delta z = \lambda_c^0/2$. The cellular pattern is visible from one wavelength λ_c^0 in figure 15. The cut was taken at $x = 6.0082$ at the peak of the total local energy production. The absence of mirror symmetry planes at $z = \text{const.} + \lambda_c^0/2$ indicates that the pattern is a travelling wave with the phase velocity $c^0 = |\omega_c^0|/k_c^0 = 0.0191$ and angular frequency $|\omega_c^0| = 0.0253$. The critical wavelength $\lambda_c^0 = 4.7377$ is approximately the same as for the centrifugal type of instability.

It is interesting to note that the instability mechanism in the range of Γ considered resembles that of the backward-facing-step flow for $0.709 \lesssim \Gamma_{BFS} \lesssim 0.9$ (Lanzerstorfer & Kuhlmann 2012*a*).

3.5. *Stationary instability for expansion ratios* $\Gamma \leqslant 0.7$

3.5.1. *Instability for* $0.35 \leqslant \Gamma \leqslant 0.7$

In the parameter range $0.35 \leqslant \Gamma \leqslant 0.7$, all integral energy production rates I_i' for $i = 1, 2, 3, 4$, are positive (see table 3 for $\Gamma = 0.5$) and thus contribute to the instability. The terms $I_2'^+$ and $I_4'^+$ are responsible for almost 83 % of all the positive energy production. However, the process I_1' exhibits the strongest maximum in the total local energy production, which makes the physical interpretation difficult.

Figure 16 shows the streamlines of the base flow and the amplitude function of the critical mode $|\hat{\boldsymbol{u}}|$ for $\Gamma = 0.5$ at critical conditions, i.e. $Re_c^0 = 790.95$ with $k_c = 0.6339$. It also depicts the spanwise vorticity of the critical mode (arrows) in a plane, in

https://doi.org/10.1017/jfm.2012.184 Published online by Cambridge University Press

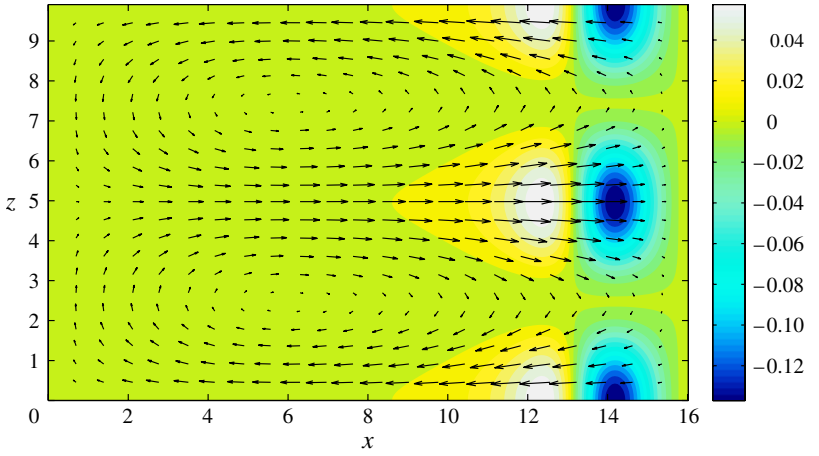


FIGURE 17. (Colour online) Basic state streamlines, perturbation flow (arrows) and the total local energy production $\sum_i I'_i$ at $y = 0.4147$ for $\Gamma = 0.5$ and $Re_c^0 = 790.95$.

which the spanwise perturbation component $\tilde{w}$ takes its maximum amplitude. It can be noticed that the amplitude of the perturbations as well as their vorticity are strongest on the downstream side of the primary vortex of the basic flow.

Figure 17 shows the critical flow pattern consisting of alternating streamwise streaks. It illustrates, moreover, that the total local energy transfer, shown at its peak $y = 0.4147$, is strongly localized at around $x \approx 12.34$ and does not extend further upstream.

In figure 18 we show the total local energy transfer rate $\sum_i I'_i$ and the above-mentioned amplification processes I'_1, I'_2 and I'_4. All terms attain their extrema in the same planes $z = \text{const}$. It can be seen from figure 18(*d*) that the critical mode gains most of its energy from I'_4 near the separating streamline where the flow is strongly decelerated. In the same region, the flow is significantly stabilized through the process I'_2 (figure 18*c*). Therefore, the term I'_1 (figure 18*b*) contributes most to the maximum in the total local energy production $\sum_i I'_i$ (figure 18*a*). The process I'_1 describes a cross-stream displacement of base flow momentum $\tilde{\boldsymbol{u}}_\perp \cdot \boldsymbol{\nabla} \boldsymbol{u}_0$, feeding back on the perpendicular perturbation $\tilde{\boldsymbol{u}}_\perp$. In order for this process to have a destabilizing effect, the orientation of $\boldsymbol{u}_0$ must change perpendicular to it, which is satisfied for the converging streamlines of the basic state.

In light of the above, we argue that in the parameter range $0.35 \leqslant \Gamma \leqslant 0.7$ the flow becomes unstable due to streamline convergence within the downstream side of the primary vortex (I'_1), in combination with flow deceleration near the reattachment point (I'_4) and an amplification process due to shear stresses near and between the primary and tertiary vortex (I'_2).

The critical mode and the mechanisms of instability for this instability are again very similar to the instability of the backward-facing-step flow for $0.4 \lesssim \Gamma_{BFS} < 0.709$ (Lanzerstorfer & Kuhlmann 2012*a*). In fact, the basic flow topology near the reattachment point of the separating streamline is the same.

3.5.2. *Shear instability for* $\Gamma < 0.35$

For small expansion ratios, a relatively high Reynolds number is required to destabilize the flow. Under critical conditions the primary vortex of the basic flow

https://doi.org/10.1017/jfm.2012.184 Published online by Cambridge University Press

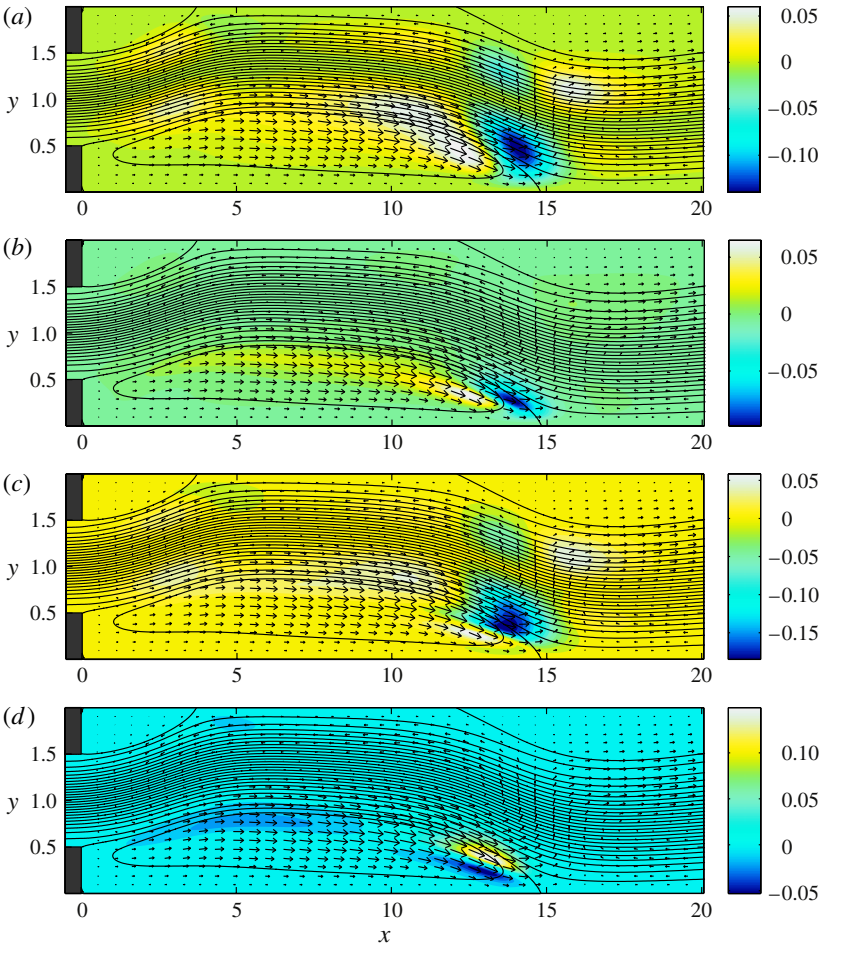


FIGURE 18. (Colour online) Basic state streamlines, critical velocity fields (arrows) and local energy production rates for $\Gamma = 0.5$ and $Re_c^0 = 790.95$. (*a*) Total local production $\sum_i I_i'$, (*b*) I_1', (*c*) I_2', and (*d*) I_4'.

is extremely stretched in the streamwise direction (figure 19). The steady and three-dimensional critical mode at $Re_c^0 = 6434.2$ with $k_c^0 = 0.1292$ for $\Gamma = 0.25$ is confined between the primary and the tertiary vortex of the basic state. The perturbation flow emerges in the form of a single vortex, which is centred at the channel centreline $y = 1$ and spanning the full outlet channel width. The effect of a corresponding finite-amplitude perturbation would be an elongation and contraction of the primary and tertiary vortex, periodic in the z-direction, which is accompanied by a straightening or bending of the jet between both separated vortices.

From figure 19 it can be observed that the disturbances gain most of their energy in two regions, being located around $x \approx 23.31$. The peak value of the production in the region near the separation point of the tertiary vortex is marginally larger than the one near the reattachment point of the primary vortex. By inspection of $I_i'^+$ (table 3), one finds that $I_2'^+$ is responsible for $\sim$87.44 % of all the positive energy production. Therefore, I_2' and $\sum I_i'$ are qualitatively the same. The same behaviour was found for the symmetry-breaking instability of the symmetric flow for $\Gamma = 0.25$ (§ 3.3).

https://doi.org/10.1017/jfm.2012.184 Published online by Cambridge University Press

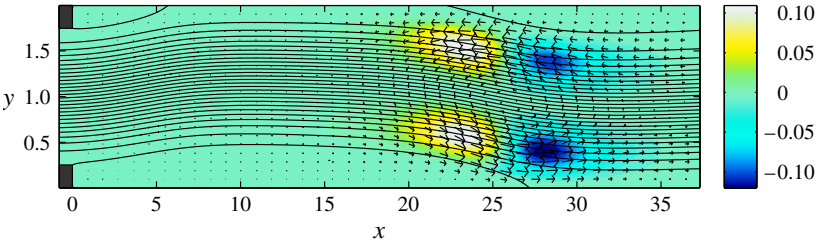


FIGURE 19. (Colour online) Basic state streamlines, perturbation flow (arrows) and the local energy production $I_2' \approx \sum I_i'$ for $\Gamma = 0.25$ and $Re_c^0 = 6434.2$. Note the scaling of the x and y axes.

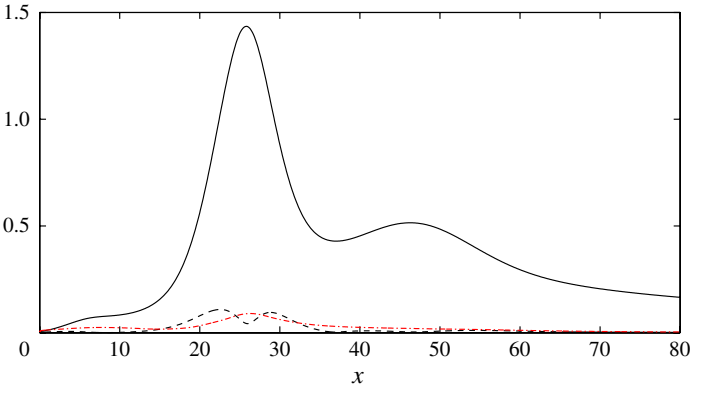


FIGURE 20. (Colour online) Amplitudes of the perturbations, integrated over the y and averaged over the z direction $\text{mean}_z \int |\tilde{\boldsymbol{u}}(x, y, z)|\,\mathrm{d}y$ for $\Gamma = 0.25$ and $Re_c^0 = 6434.2$. The solid, dashed and the dash-dotted (red) line represent the $\tilde{u}$, the $\tilde{v}$ and the $\tilde{w}$ component, respectively. The outlet is located at $x = 400$.

To demonstrate the streamwise distribution of the strength of the perturbation flow, figure 20 shows the amplitudes of the critical velocity field by components, integrated over y and averaged over z, i.e. $\text{mean}_z \int |\tilde{\boldsymbol{u}}(x, y, z)|\,\mathrm{d}y$. It can be seen that the spanwise perturbation velocity component $\tilde{w}$ is rather weak. This result is consistent with the fact that the critical wavelength $\lambda_c^0 = 48.63$ is extremely long.

Owing to the similarities of the critical modes and its associated energy transfer rates for the symmetric and the asymmetric basic flows (compare figures 19 and 10), we think that shear is mainly responsible for the instability for $\Gamma < 0.35$.

3.6. *Comparison with experiments*

The flow in a symmetric duct with an expansion ratio of $\Gamma = 0.5$ and a spanwise aspect ratio of $\Lambda = d/h_i = 8$ (depth-to-height of the inflow channel) was analysed by Cherdron *et al.* (1978) using flow visualizations and laser Doppler anemometry measurements. Their experiments revealed that the flow was symmetric for $Re = 150$, but asymmetric for $Re = 185$. Moreover, it was reported that, for $Re \geqslant 800$ onwards, the flow became very disturbed, with large longitudinal velocity fluctuations. The experiments of Durst *et al.* (1993) for $\Gamma = 0.5$ and $\Lambda = 16$ predicted that symmetry-breaking bifurcation would occur at around $Re_c^{2D} \approx 125$. Further, it was reported

https://doi.org/10.1017/jfm.2012.184 Published online by Cambridge University Press

that the fully laminar regime reaches up to $Re \leqslant 610$, which was the highest Reynolds number considered. Our global, temporal linear stability results predicted that symmetry-breaking bifurcation would occur at $Re_c^{2D} = 216.76$. The discrepancy with the aforementioned experimental results of Cherdron *et al.* (1978) and Durst *et al.* (1993) might be put down to the finite spanwise aspect ratios Λ. Apparently, Λ was too small to sufficiently prevent end effects in the experiments. This explanation is also supported by Tsui & Wang (2008), who showed that for a spanwise aspect ratio of $\Lambda \geqslant 24$ side-wall effects can be neglected and the flow can be regarded as two-dimensional at the centreline $z = 0$. Nevertheless, the stability boundary for the asymmetric flow solution $Re_c^0 = 790.94$ is consistent with the experiments of Cherdron *et al.* (1978) with $Re_c^{Ch} \approx 800$.

The flow visualizations and laser Doppler anemometry measurements of Durst *et al.* (1974) revealed that the flow is symmetric for $Re = 84$, but asymmetric for $Re = 171$ for $\Gamma = 0.\dot{6}$ and $\Lambda = 27.5$. They also reported that the flow became very disturbed within the separation zones for $Re \geqslant 439.5$. For approximately the same geometry, i.e. $\Gamma = 0.\dot{6}$ and $\Lambda = 24$, experiments were carried out by Fearn *et al.* (1990). They could not detect any symmetric solution for $Re \geqslant 105$. It was shown, moreover, that the flow remained steady up to $Re \leqslant 453$ and the flow became unsteady as a consequence of three-dimensional effects for higher Reynolds number. These experimental results of Durst *et al.* (1974) and Fearn *et al.* (1990) agree quite well with our findings, yielding an exchange of stability at $Re_c^{2D} = 121.74$ and a loss of stability of the asymmetric flow for $Re_c^0 \geqslant 454.83$.

4. Conclusions

The global, temporal linear stability of the two-dimensional, incompressible flow in a plane sudden expansion has been analysed for a quasi-continuous variation of the expansion ratio Γ. The influence of the in- and outlet channel lengths on the stability boundaries has been analysed to obtain results, independent of these two external parameters. In addition, the flow stability for an asymmetric expansion with $\alpha = 0.15$ has been investigated. It turned out that the flow structure of the slightly non-symmetric geometry resembles the asymmetric flow solution of the symmetric geometry. Also, the stability boundaries of these two systems are almost congruent. Therefore, the main effect for a slightly asymmetric expansion is to shift the disconnected branches to higher Reynolds numbers.

The analysis has shown that the critical Reynolds numbers Re_c are monotonically decaying functions of the expansion ratio Γ. By using a definition of the Reynolds number based on a scaling which depends only on the upstream conditions, Re_c^* scales linearly for very large step heights $(1 - \Gamma) \ll 1$. We find that the critical Reynolds number for the primary symmetric flow is significantly below that of the secondary asymmetric flow solution.

Our results confirm previous works showing that the primary instability is two-dimensional, stationary, and breaks the mirror symmetry with respect to the channel mid-plane. Using an *a posteriori* energy transfer analysis we find that the primary instability is due to a combination of flow deceleration and shear for large expansion ratios. For small expansion ratios, the role of flow deceleration diminishes, and the instability is due to shear.

In addition to the primary instability, we have computed, for the first time, the secondary instability. The instability of the asymmetric flow solution is generally three-dimensional. Even though two-dimensional and time-dependent neutral modes

https://doi.org/10.1017/jfm.2012.184 Published online by Cambridge University Press

exist (as anticipated by Cherdron *et al.* 1978 and Durst *et al.* 1993), they are never the most dangerous ones. Typically, the neutral Reynolds number for two-dimensional time-dependent perturbations is at least twice the (three-dimensional) critical Reynolds number. For $\Gamma = 0.93$ we find, for example, $Re_n^0(k = 0) = 1167$ with $\omega_n^0(k = 0) = 0.476$ and for $\Gamma = 0.95$ we obtain $Re_n^0(k = 0) = 1023$ with $\omega_n^0(k = 0) = 0.393$.

The three-dimensional instabilities are due to different physical mechanisms, depending on the expansion ratio. For small expansion ratios $\Gamma \leqslant 0.35$, the instability of the finite-amplitude two-dimensional asymmetric flow is stationary and similar to the primary instability. The critical three-dimensional, long-wave mode is almost mirror symmetric with respect to the mid-plane, and it is caused by shear stresses. For moderate step heights $0.35 \leqslant \Gamma \leqslant 0.7$ the critical mode is still stationary, but the instability cannot be attributed to a particular type of energy transfer process, because different mechanisms work together. In particular, the combined effects of flow deceleration near the reattachment point, an amplification process due to shear on both edges of the plane jet, and streamline convergence within the downstream region of the separated flow has a destabilizing effect. As the expansion is further increased, i.e. for $\Gamma \geqslant 0.713$, the critical mode changes from stationary to oscillatory. At $\Gamma \approx 0.8$ the disturbances gain their entire energy from the central region of the strained primary vortex. The energy transfer characteristics and the structure of the critical perturbation flow indicate that the nature of the instability is of elliptic type. For even higher expansion ratios, the oscillatory critical mode and the energy transfer characteristics change continuously until centrifugal forces prevail for very large step heights $(1 - \Gamma) \ll 1$. In this situation the local energy production and the perturbations are most pronounced in those regions where the plane jet of the basic flow is curved, just before its oblique impingement on the walls. There exist two zones with equivalent flow structures and energy production zones on the concave side of the curved jet. The first zone is located in the curved jet just before its first impingement and the second zone is located in the curved separated jet just before the second impingement. These local flow conditions, and also the criterion of Sipp & Jacquin (2000), suggest that the flow becomes centrifugally unstable.

It is worth mentioning that the topology of the asymmetric critical modes ($\Gamma \gtrsim 0.4$) and their associated instability mechanisms are very similar to those studied by Lanzerstorfer & Kuhlmann (2012*a*) in the backward-facing-step problem. These analogies seem to be due to the basic flows which are locally very similar in both systems.

The physical relevance of the global instability modes found is established by demonstrating the consistency with previous experimental findings. The numerical results are consistent with the experimental data regarding the primary symmetry-breaking bifurcation. Moreover, qualitative agreement is obtained for critical data of the secondary instability. In view of the remaining differences between numerical and experimental threshold data it would be worthwhile to carry out more accurate experiments in which the perturbing influence of the end walls is substantially minimized.

Appendix

Table 4 summarizes the critical Reynolds, wavenumbers and oscillatory frequencies for several expansion ratios, which might provide useful reference data for further investigations. Note that the critical parameters are scaled according to (2.4). Also, the

https://doi.org/10.1017/jfm.2012.184 Published online by Cambridge University Press

Γ	Re_c^{2D}	L_o	N_x^o	N_x^i	N_y^i	N_y^o
0.25	1657.7	126	1771	223	116	192
0.3	934.83	78	1119	212	112	200
0.4	394.87	34	522	190	104	212
0.5	216.76	25	399	169	94	218
0.6	144.96	20	331	147	82	222
$0.\dot{6}$	121.74	20	331	132	74	222
0.7	114.59	10	196	125	70	222
0.8	107.11	10	196	103	54	218
0.9	130.17	10	196	80	32	208
0.95	188.47	10	196	59	18	202

Γ	Re_c^0	k_c^0	$\lvert\omega_c^0\rvert$	Re_c^α	k_c^α	$\lvert\omega_c^\alpha\rvert$	L_o	N_x^o	N_x^i	N_y^i	N_y^o
0.25	6434.2	0.1292	0	6319.5	0.1294	0	400	5491	223	116	192
0.3	3789.5	0.1421	0	3728.4	0.1427	0	320	4405	212	112	200
0.4	1569.5	0.4766	0	1542.1	0.5301	0	130	1825	190	104	212
0.5	790.95	0.6339	0	774.43	0.6715	0	65	943	169	94	218
0.6	513.31	0.8064	0	503.91	0.8249	0	40	603	147	82	222
$0.\dot{6}$	454.83	0.9683	0	447.81	0.9713	0	40	603	132	74	222
0.7	445.80	1.1726	0	441.13	1.1571	0	35	535	125	70	222
0.8	375.98	1.3262	0.0253	374.16	1.3413	0.0259	25	399	103	54	218
0.9	370.53	1.3066	0.0456	373.65	1.3492	0.0470	15	264	80	32	208
0.95	423.48	1.3031	0.0485	430.85	1.3582	0.0509	15	264	59	18	202

TABLE 4. Critical parameters for the scaling (2.4) for selected expansion ratios Γ, the outflow length L_o and the number of grid points (N_x, N_y) in the (x, y)-plane.

outflow length L_o and the number of grid points used are indicated. N_x^i and N_y^i stand for the numbers of grid points in the x- and y-directions in the inflow channel, while N_x^o and N_y^o represent those for the outflow channel. Thus the last five columns specify the geometry parameters.

REFERENCES

ALLEBORN, N., NANDAKUMAR, K., RASZILLIER, H. & DURST, F. 1997 Further contributions on the two-dimensional flow in a sudden expansion. *J. Fluid Mech.* **330**, 169–188.

BATTAGLIA, F., TAVENER, S. J., KULKARNI, A. K. & MERKLE, C. L. 1997 Bifurcation of low Reynolds number flows in symmetric channels. *AIAA Journal* **35** (1), 99–105.

BAYLY, B. J. 1988 Three-dimensional centrifugal-type instabilities in inviscid two-dimensional flows. *Phys. Fluids* **31**, 56–64.

CHERDRON, W., DURST, F. & WHITELAW, J. H. 1978 Asymmetric flows and instabilities in symmetric ducts with sudden expansions. *J. Fluid Mech.* **84** (1), 13–31.

CHIANG, T. P., SHEU, T. W. H., HWANG, R. R. & SAU, A. 2001 Spanwise bifurcation in plane-symmetric sudden-expansion flows. *Phys. Rev.* E **65**, 1–16.

CHIANG, T. P., SHEU, T. W. H. & WANG, S. K. 2000 Side wall effects on the structure of laminar flow over a plane-symmetric sudden expansion. *Comput. Fluids* **29**, 467–492.

DRIKAKIS, D. 1997 Bifurcation phenomena in incompressible sudden expansion flows. *Phys. Fluids* **9** (1).

DURST, F., MELLING, A. & WHITELAW, J. H. 1974 Low Reynolds number flow over a plane symmetric sudden expansion. *J. Fluid Mech.* **64** (1), 111–128.

DURST, F., PEREIRA, J. C. F. & TROPEA, C. 1993 The plane symmetric sudden-expansion flow at low Reynolds numbers. *J. Fluid Mech.* **249**, 567–581.

https://doi.org/10.1017/jfm.2012.184 Published online by Cambridge University Press

FEARN, R. M., MULLIN, T. & CLIFFE, K. A. 1990 Nonlinear flow phenomena in a symmetric sudden expansion. *J. Fluid Mech.* **211**, 595–608.

HAWA, T. & RUSAK, Z. 2000 Viscous flow in a slightly asymmetric channel with a sudden expansion. *Phys. Fluids* **12** (9), 2257–2267.

HAWA, T. & RUSAK, Z. 2001 The dynamics of a laminar flow in a symmetric channel with a sudden expansion. *J. Fluid Mech.* **436**, 283–320.

KUHLMANN, H. C. 1999 *Thermocapillary Convection in Models of Crystal Growth*, *Springer Tracts in Modern Physics*, vol. 152. Springer.

LANZERSTORFER, D. & KUHLMANN, H. C. 2012*a* Global stability of the two-dimensional flow over a backward-facing step. *J. Fluid Mech.* **693**, 1–27.

LANZERSTORFER, D. & KUHLMANN, H. C. 2012*b* Three-dimensional instability of the flow over a forward-facing step. *J. Fluid Mech.* **695**, 390–404.

LEHOUCQ, R. B. & SORENSEN, D. C. 1996 Deflation techniques for an implicitly restarted Arnoldi iteration. *SIAM J. Matrix Anal. Appl.* **17**, 789–821.

MIZUSHIMA, J. & SHIOTANI, Y. 2000 Structural instability of the bifurcation diagram for two-dimensional flow in a channel with a sudden expansion. *J. Fluid Mech.* **420**, 131–145.

PIERREHUMBERT, R. T. 1986 Universal short-wave instability of two-dimensional eddies in an inviscid fluid. *Phys. Rev. Lett.* **57**, 2157–2159.

RUSAK, Z. & HAWA, T. 1999 A weakly nonlinear analysis of the dynamics of a viscous flow in a symmetric channel with a sudden expansion. *Phys. Fluids* **11** (12), 3629–3636.

SCHRECK, E. & SCHÄFER, M. 2000 Numerical study of bifurcation in three-dimensional sudden channel expansions. *Comput. Fluids* **29** (5), 583–593.

SHAPIRA, M. & DEGANI, D. 1990 Stability and existence of multiple solutions for viscous flow in suddenly enlarged channels. *Comput. Fluids* **18** (3), 239–258.

SHTERN, V. & HUSSAIN, F. 2003 Effect of deceleration on jet instability. *J. Fluid Mech.* **480**, 283–309.

SIPP, D. & JACQUIN, L. 1998 Elliptic instability in two-dimensional flattened Taylor–Green vortices. *Phys. Fluids* **10**, 839–849.

SIPP, D. & JACQUIN, L. 2000 Three-dimensional centrifugal-type instabilities of two-dimensional flows in rotating systems. *Phys. Fluids* **12**, 1740–1748.

SOBEY, I. J. & DRAZIN, P. G. 1986 Bifurcations of two-dimensional channel flows. *J. Fluid Mech.* **171**, 263–287.

SQUIRE, H. B. 1933 On the stability of three-dimensional disturbances of viscous flow between parallel walls. *Proc. R. Soc. Lond.* A **142**, 621–628.

TSUI, Y.-Y. & WANG, H.-W. 2008 Side-wall effects on the bifurcation of the flow through a sudden expansion. *Intl J. Numer. Meth. Fluids* **56**, 167–184.

WALEFFE, F. 1990 On the three-dimensional instability of strained vortices. *Phys. Fluids* **2**, 76–80.

https://doi.org/10.1017/jfm.2012.184 Published online by Cambridge University Press